Available online at www.sciencedirect.com

ScienceDirect

Energy Procedia 45 (2014) 207 – 216

Energy Procedia

68th Conference of the Italian Thermal Machines Engineering Association, ATI2013

Performance and flow field evaluation of a Savonius rotor tested in a wind tunnel

Marco Torresi[a,*], Fabio A. De Benedittis[a], Bernardo Fortunato[a], Sergio M. Camporeale[a]

[a]*Department of Mechanics, Mathematics and Management (DMMM), Politecnico di Bari, Via Re David, 200, Bari 70125, Italy*

Abstract

A renewed interest on Vertical Axis Wind Turbines (*VAWTs*) arose from their great capacity for integration within urban areas and for applications of distributed generation. In order to be able to highly improve their performance, making them competitive with respect to the more consolidated Horizontal Axis Wind Turbines (*HAWTs*), it is fundamental to have a deeper comprehension of their fluid dynamic behavior. In order to reach this goal, a two-bucket Savonius rotor has been designed, built from a *PVC* pipe with a nominal diameter of 200 *mm*, and tested in the wind tunnel of the Department of Mechanics, Mathematics and Managment (*DMMM*) of the Politecnico di Bari. The Savonius rotor is connected to an AC brushless servo motor, able to control either the braking torque or the rotational speed. This paper describes the experimental evaluation of the unsteady flow field downstream the rotor by means of a Constant Temperature hot wire Anemometer (*CTA*). Whilst, for performance analysis, the torque measurements have been obtained directly from the Servo Amplifier torque monitor.

Selection and peer-review under responsibility of ATI NAZIONALE

Keywords: Vertical Axis Wind Turbines; Savonius Rotor; Wind Tunnel tests; wake analysis; Hot Wire Constant Temperature Anemometry.

1. Introduction

Actually, the power sector is responsible for more than 40% of all carbon dioxide (CO_2) emissions from burning fossil fuels, and about 25% of the total greenhouse gas (*GHG*) emissions [1]. The main way to significantly reduce carbon dioxide emissions in the power sector is the use of renewable energy.

Nomenclature

a	equivalent overlap, (*mm*)
C_m	torque coefficient

* Corresponding author. Tel.: + 39 080 5963577; fax: + 39 080 5963411
E-mail address: m.torresi@poliba.it

Selection and peer-review under responsibility of ATI NAZIONALE
doi:10.1016/j.egypro.2014.01.023

Nomenclature

D	rotor diameter, (mm)
D_o	end plate diameter, (mm)
D_s	shaft diameter, (mm)
f	fan frequency, (Hz)
H	rotor height, (mm)
I_o	moment of inertia of the Savonius rotor, (kgm^2)
n	turbine rotational speeds, (rpm)
R_e	external radius of the buckets, (mm)
s	thickness of the buckets, (mm)
SR	sampling rate, (Hz)
θ	azimuth angle, (deg)
λ	tip speed ratio
ρ_{PVC}	PVC density, (kg/m^3)

Among renewables, wind energy is actually the largest contributor, which has reduced global emissions by about 400 million tonnes in 2012 [1]. This result is confirmed by the annual global market trend, according to which, in 2012, a wind power installation growth of about $45\,GW$ (i.e. 10% with respect to the cumulative installation up to 2011) has been registered. These data, associated with cumulative market growth of almost 19%, mean that 2012 ended with $282.5\,GW$ of global installed wind power [2]. In 2012, wind-generated electricity in China amounted to $100.4\,TWh$, accounting for 2% of the country's total electricity output, and wind energy was the third largest source of electricity after thermal and hydropower in China, surpassing nuclear during the course of the year. Also, wind energy was the largest source of new US electricity generation in 2012, providing some 42% of all new capacity [2]. Wind energy represented 26% of all new European Union's (EU) power capacity installed in 2012, the second biggest share after solar PV (37%) and before gas (23%) [3]. Wind is now meeting 7% of Europe's electricity demand, up from 6.3% at the end of 2011 and 4.8% in 2009. In particular, during 2012, $11.895\,GW$ of wind power capacity was installed in the EU ($10.729\,GW$ onshore and $1.166\,GW$ offshore) whilst renewable power installations accounted for 70% of all new installations (actually $31.3\,GW$ out of $44.9\,GW$). In the same year in the EU, wind energy have reached a total of installed power equal to $106\,GW$ with a growth of 12.6% on the previous year and similar to the growth recorded in 2011 [3]. So, there is a strong expectation for wind power technology and its development for next years, in particular greater importance are gaining small wind turbines up to $100\,kW$ for their use in: urban environments (commercial and residential areas), hybrid systems, pumping [4]. The world market for small wind has seen further strong growth: at the end of 2011, a cumulative total of at least 730000 small wind turbines were installed all over the world, 74000 of which were newly erected just in 2011. During 2011, the number of installed small wind turbines grew by 11%. Small wind capacity has reached more than $576\,MW$ at the end of 2011 with a global capacity increase of 27% [4]. The main reason for the small wind turbine technology development is the possibility to install small units that can work where the wind power is very concentrated but not enough [5]. This paper focuses its attention on a particular vertical axis wind turbine ($VAWT$): the Savonius rotor (see Fig. 1). The Savonius rotor is a drag driven device used for the conversion of wind energy into mechanical energy made available at the shaft. Invented by the Finnish engineer Sigurd J. Savonius in 1922 and patented in 1929, the Savonius rotor is one of the simplest wind turbines: actually it can be built by halving a pipe, and then shifting the two semi-cylindrical surfaces along the cutting plane so as to resemble the letter S [6]. The rotor therefore consists, in its most simple form, of two buckets, hinged on the rotor shaft. Erroneously the Savonius rotor is sometime confused with the real S rotor: the fundamental difference between these two wind turbines is given by the presence of a gap (said overlap) between the two buckets in the case of Savonius rotors, absent in the case of S rotors. The bucket overlap changes the velocity field through the machine allowing the buckets to increase the shaft torque by lift contributions and moving the optimum tip speed ratio (TSR or λ) beyond 1, making the Savonius rotor definitely more efficient, whereas purely drag driven turbine can hardly go further $\lambda = 1$. Being mainly a drag driven device, aerodynamic theories, developed in order to

analyze lift driven wind turbines, cannot be applied in the case of Savonius rotors. This means that wind tunnel tests and computational fluid-dynamics are the only tools available for studying Savonius rotors ([7]-[10]).

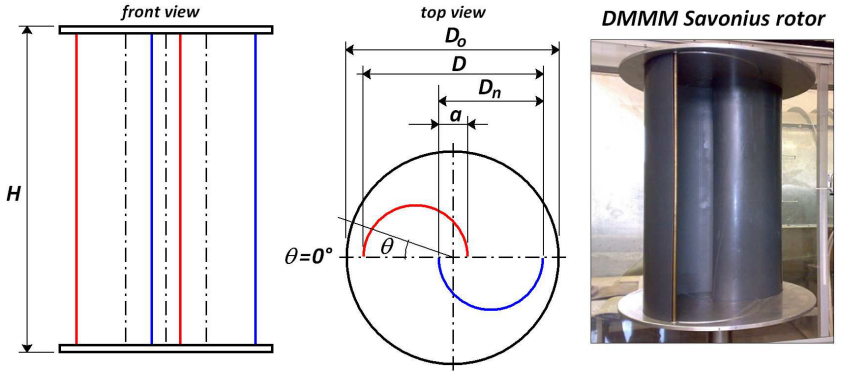

Fig. 1. *DMMM* Savonius Rotor

The interest for such a turbine is due to the following consideration: despite Savonius rotors have lower performance compared to horizontal axis wind turbines (*HAWTs*), they have the advantage to be able to capture wind energy independently from the wind direction. The average rated capacity of *VAWTs* is estimated to be $7.4\,kW$ with a median rated capacity of $2.5\,kW$, while for *HAWTs* average and median rated capacity are $10.8\,kW$ and $3.0\,kW$, respectively [3]. However *VAWTs* (and Savonius in particular) presents the following advantages: high starting torque, extremely low cut-in speed, easy on-site manufacturing using on-site materials [11] [12], self-starting, very low noise level. So, for this reasons, *VAWTs* can be more suitable for commercialization. The aim of this work is to gain an insight into the complex flow field through Savonius rotors and to evaluate the performance of such a turbine.

2. Experimental apparatus

Experiments have been carried out in the subsonic, closed-loop, wind tunnel of the Politecnico di Bari (see Fig. 2). The maximum air speed that can be reached in the test section is equal to $40\,m/s$. Thanks to the aerodynamic blades introduced in the two wind tunnel curves and the honeycomb placed upstream the convergent duct (characterized by a shrink factor 4:1), the velocity distribution is uniform and characterized by a low turbulence level. The axial fan, driven by a $55\,kW$ electric asynchronous motor, provides the kinetic energy to the air-flow in order to preserve the flow in the tunnel.

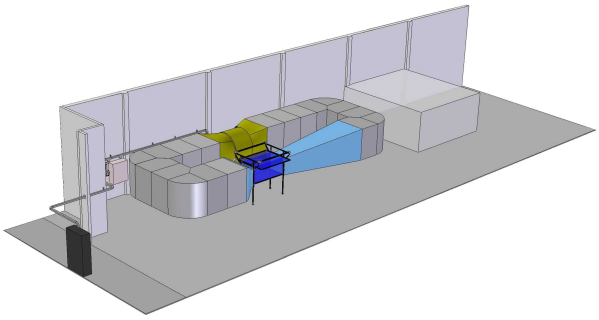

Fig. 2. *CAD* of the wind tunnel at *DMMM*

The test section is $2.32\,m$ long with a $1x1\,m^2$ cross-section, made of transparent polycarbonate sheets connected by an aluminum frame. The Savonius rotor is located $1.15\,m$ downstream the convergent duct and centered with respect to the test chamber. Above the test section, in order to accurately position the hot wire probe for velocity

measurements, there is a three-axis Cartesian robot, equipped with four motors driven by bipolar steppers (see Fig. 3). In this way an experimental grid in any vertical or horizontal plane can be defined in order to analyze the flow-field.

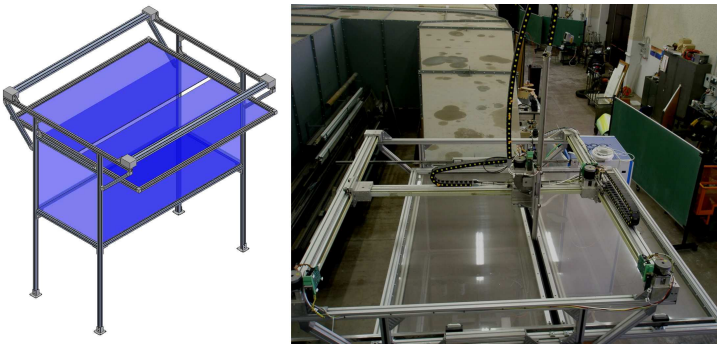

Fig. 3. Test section and structure of the Cartesian robot of the wind tunnel at *DMMM*

The wind tunnel is equipped with: hardware for system control; acquisition and data processing systems; one PC with A/D and digital interface boards; $RS\,232/RS\,422/RS\,485$ serial interface boards for managing the communication via modbus protocol with the inverter, which drives the circulation fan; a LabVIEW environment for data acquisition and processing; a data storing system with a removable hard disk. The entire control and acquisition system was implemented using: a single workstation, National Instruments (*NI*) data acquisition boards (*DAQ*), a motion control system, and a Constant Temperature Anemometer (*CTA*) hardware. Torque measurements are redundantly obtained from both a load cell (connected to the cradling case of the brushless motor) and the brushless servo amplifier. All the actions (e.g. turbine speed control, three-axis traversing motion control for the *CTA* probe; circulation fan control; and tunnel safety interlock definition) are remotely controlled by a virtual instrument (*VI*) developed under LabVIEW environment.

3. Savonius Rotor

The Savonius rotor prototype under investigation has been built at the *DMMM* Lab [13] with two semicircular buckets (see Fig. 1) obtained by halving a $D_n = 200\,mm$ *PN6 PVC* pipe. *PVC* is a material characterized by low specific weight (its density is $\rho_{PVC} = 1450\,kg/m^3$), good mechanical strength, relatively low cost and easy machinability. The external bucket radius is $R_e = 100\,mm$ and its thickness is $s = 4.9\,mm$, the rotor height is $H = 412\,mm$. The shaft diameter is $D_s = 20\,mm$, hence the equivalent overlap is $a = 40.2\,mm$. The rotor diameter is $D = 330\,mm$, while the end plate diameter has been chosen to be $D_o = 360\,mm$. The moment of inertia of the entire Savonius rotor is $I_o = 0.0816\,kgm^2$.

4. Results

Results are given in terms of turbine performance (actually torque coefficient, C_m, vs. tip speed ratio, λ, and shaft torque polar diagram) and flow-field analyses.

4.1. Performance

In order to evaluate the global performance of the Savonius rotor, the shaft torque has been measured (reading its value directly from the Servo Amplifier torque monitor) under different flow conditions (wind speed equal to 6, 7 and $8\,m/s$, respectively) during the flow-field acquisitions, with the turbine rotating at $n = 300\,rpm$ and the circulating fan driven at $f = 8\,Hz$. In Fig. 4 the torque coefficient, C_m, and the power coefficient, C_p, have been plotted vs. tip speed ratio, λ. The torque coefficient decreases almost linearly with the increase of the tip speed ratio. However, at small tip speed ratios (less than 0.3), this is no more true, since the turbine has a small rotational speed with respect to the

wind speed and hence the shed vortices intensely interact with the turbine buckets lowering their performance. The maximum power coefficient is equal to 0.21 for $\lambda = 0.8$.

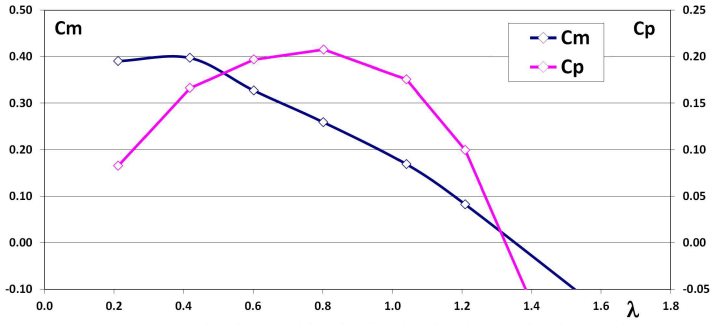

Fig. 4. Torque coefficient, C_m, vs. tip speed ratio, λ, at different wind speeds

In Fig. 5 the polar diagram of the phase-averaged shaft torque (measured at $n = 300\,rpm$ and $f = 8\,Hz$) is reported, evidencing the typical bilobed shape. This data have been subject to a filtering operation for smoothing, using the simplified least squares procedures proposed by Savitzky and Golay [14], which is characterized by a very limited distortion into the recorded data. Even if the rotor is characterized by a geometrical symmetry of 180°, this is not the case for the shaft torque, which reveals a lack of symmetry, hence the actual angular periodicity is 360°.

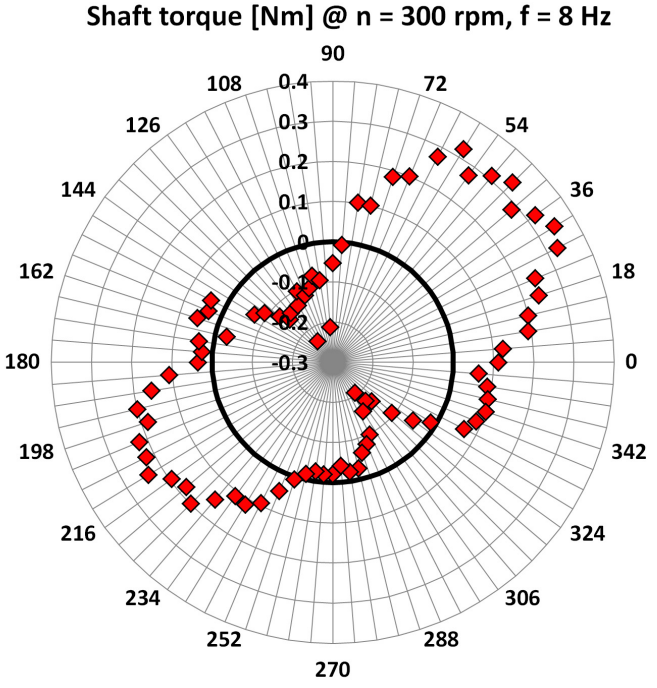

Fig. 5. Polar diagram of the Savonius rotor shaft torque at $n = 300\,rpm$ and $f = 8\,Hz$ - phase-averaged data

The main reason for a lack of periodicity every half revolution is to be found in the complex interaction of the vortex shedding with the rotating buckets. In particular the vortices interact with the bucket surfaces in different ways every 180°. The rotor experiences the maximum torque values for azimuth positions, θ, in the range $27° - 63°$ and in the range $198° - 225°$, whereas the minimum torque values are achieved in the range $99° - 126°$ and at $\theta = 306°$.

As a matter of fact, when the buckets are almost perpendicular with respect to the free stream velocity, even if the advancing bucket is giving the highest torque contribution, the returning bucket is actually giving its strongest adverse contribution. Conversely, when the buckets are almost aligned with respect to the free stream velocity, the advancing bucket gives a minimum resistant contribution to rotation; whereas the returning bucket, thanks to the flow passing through the overlap passage, experiences a positive lifting action maximizing the torque.

4.2. Flow field measurements

The flow field measurements have been carried out defining different investigation planes (see Fig. 6). At first, a vertical grid (600 mm x 772 mm) with 81 points (9 points with a mesh size $\Delta X = 96.5\,mm$ along X-axis, and 9 points with a mesh size $\Delta Z = 75\,mm$ along Z-axis) has been defined (see Fig. 7) where placing the hot wire probe. This vertical grid has been used for two different planes, 1.150 m upstream and 0.850 m downstream the rotor, respectively, in order to analyze the two different flow fields (see Fig. 7). Actually, the probe is the Dantec *55P11* single-sensor miniature wire probe (5 μm thick, 1.25 mm long platinum-plated tungsten wire sensors). The wire is welded directly onto the prongs and the entire wire length acts as a sensor. The probe body is a 1.9 mm diameter ceramic tube, equipped with gold-plated connector pins that connect to the probe supports by means of plug-and-socket arrangements.

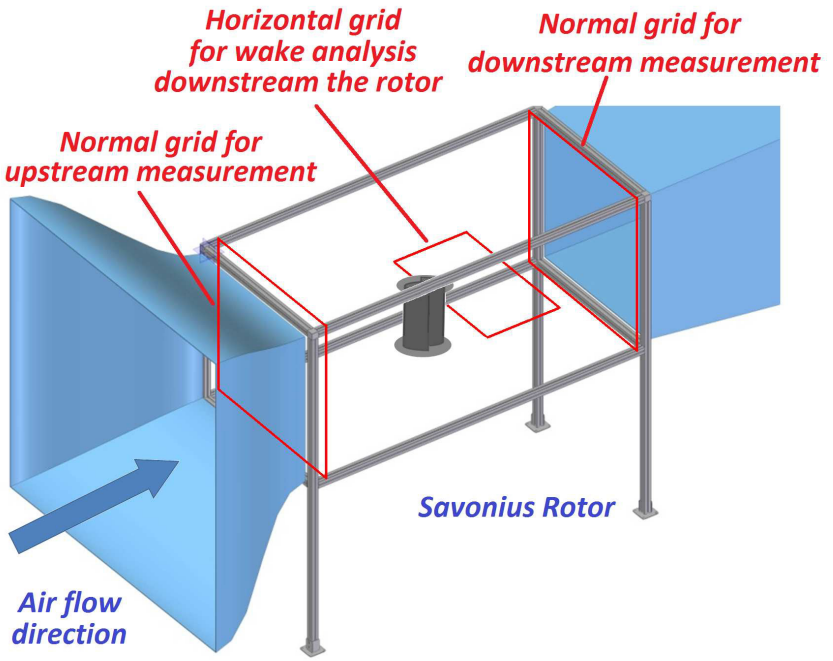

Fig. 6. Position of the investigation planes

Being the sensor a single component probe, only the streamwise velocity distribution has been considered. The flow field measurements have been carried out at constant turbine rotational speed, $n = 300\,rpm$, with a fan frequency $f = 8\,Hz$. In order to investigate the rotor wake, a grid on a horizontal plane 220 mm downstream the rotor and at its midspan has been defined (see Fig. 7). The horizontal grid is characterized by 13 points with a mesh size $\Delta X = 64.3\,mm$ along X-axis, and 16 points with a mesh size $\Delta Y = 22.2\,mm$ along Y-axis).

The acquisition system has been configured in order to investigate the unsteady behaviour of the wake downstream the rotor. Since the *CTA* acquires velocity data in a single point at a time, in order to have unsteady flow-field measurements, a phase averaged technique must be implemented. Since the servo motor, used as dynamometer, has a very accurate absolute position encoder, its signal has been used for triggering. Actually, data have been acquired every 4.5°, which means 80 sample per revolution. During the tests, the turbine rotated at $n = 300\,rpm$, which means

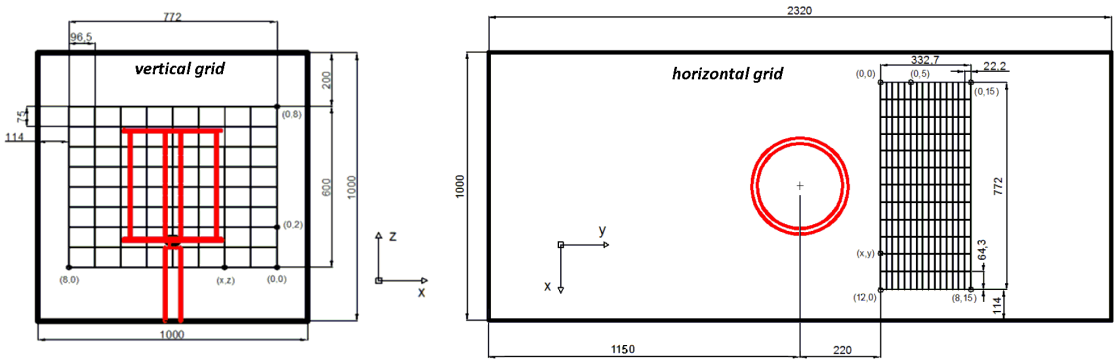

Fig. 7. Vertical (left) and horizontal (right) grids for *CTA* probe positioning

0.2 s per revolution, giving a sampling rate, $SR = 400\,Hz$. In order to perform phase averaging, 105 revolutions have been performed during each acquisition, which means 8400 available data. In order to evaluate the averaged velocity field upstream and downstream the rotor, this sampling rate has been firstly considered. Fig. 8 shows the averaged velocity fields upstream and downstream the rotor. They are not uniform and are characterized by higher values outside toward the test chamber walls, whilst they have lower values in correspondence of the central zone, i.e. where the turbine exerts the highest blockage effect. From the streamwise velocity distributions, both upstream and downstream, a lack of symmetry can be put in evidence. Actually, downstream the velocity are higher on the advancing bucket side (negative x coordinates) than on the returning side (positive x coordinates). This is due to the effect of the turbine rotation.

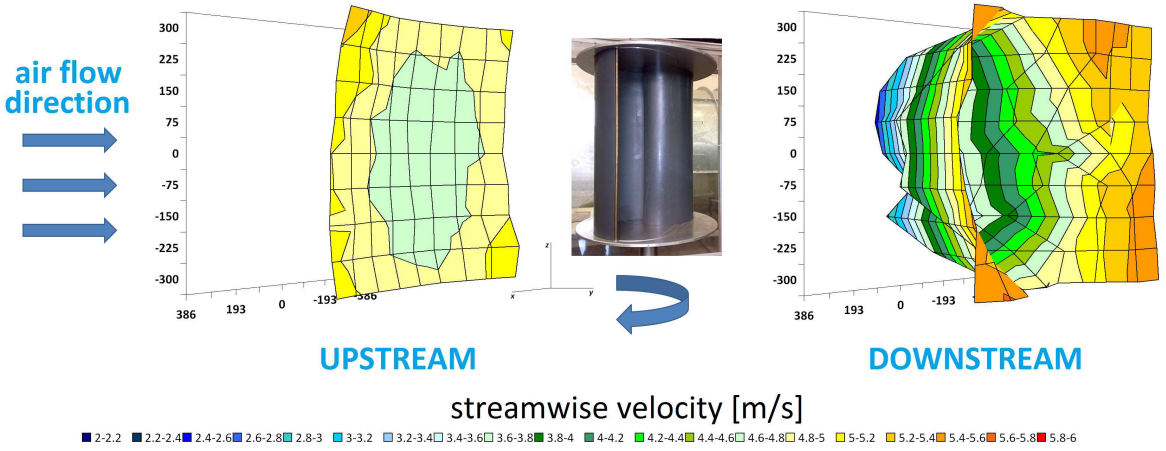

Fig. 8. Phase-averaged flow field distribution, triggered acquisition every 4.5° of turbine rotation at $n = 300\,rpm$ and $f = 8\,Hz$

In order to investigate the turbine behavior in the frequency domain, the acquisition technique has been changed. This time, measurements have been performed continuously and independently from the rotor angular position, with a sampling rate, $SR = 1kHz$. In this way, it is possible to characterized the flow field in each point of the grid with a greater number of data per point. First of all, the averaged velocity field upstream and downstream the rotor have been computed again. As expected, the two different tests essentially lead to the same results (see Fig. 9). In order to confirm the qualitative conclusion based on the comparison of Figures 8 and 9, in Fig. 10 the averaged streamwise velocity distributions along horizontal and vertical symmetry lines upstream and downstream the rotor are shown.

During the turbine rotation at 300 rpm with the fan driven at a frequency $f = 8\,Hz$, the sampled signal has been analysed in the frequency domain (see Fig. 11) applying a *DFFT* (Discrete Fast Fourier Transform). As expect, the

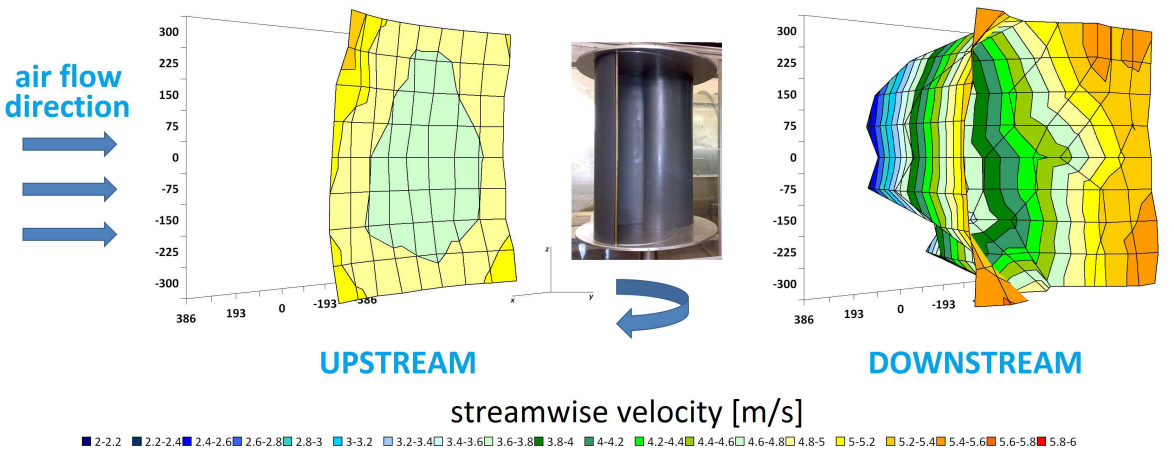

Fig. 9. Flow field distribution, continuous acquisition at 1 kHz at $n = 300\,rpm$ and $f = 8\,Hz$

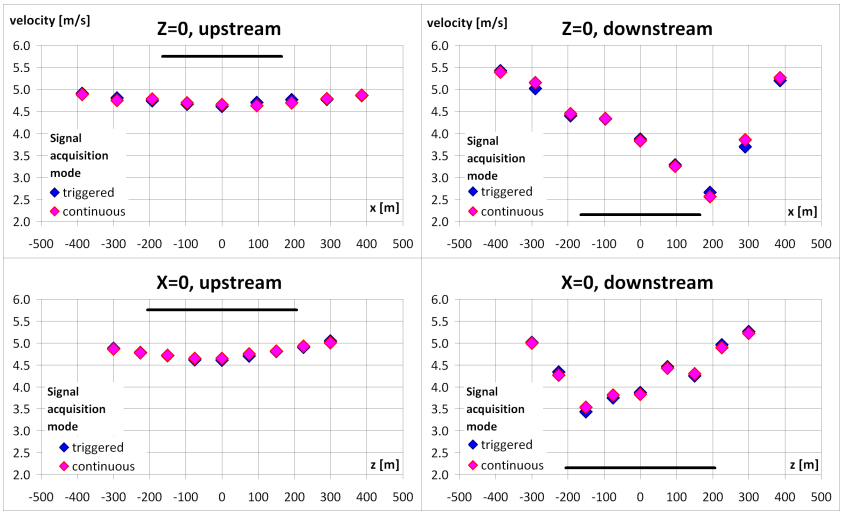

Fig. 10. Averaged streamwise velocity distribution along horizontal and vertical symmetry lines upstream and downstream the rotor ($n = 300\,rpm$, $f = 8\,Hz$)

analysis has shown a main amplitude peak at 10 Hz and a secondary peak at 20 Hz. These peaks are actually related to the rotor bucket passages, since the turbine rotates at 300 rpm (5 Hz) and has two buckets.

In order to perform the wake analysis, the fan has been driven at a frequency $f = 8\,Hz$ and the turbine has been kept rotating at $n = 300\,rpm$. Under these operating conditions the tip speed ratio, λ, was equal to 1.04. Flow visualizations have been computed by means of a phase-averaged technique applied to data collected each time over a period of time equal to 105 rotor revolutions. Fig. 12 shows the phase-averaged streamwise velocity distributions in the rotor wake during half revolution, every 18° from $\theta = 0°$, up to $\theta = 180°$, plus at $\theta = 270°$. The vortices generated in the rotor wake are shed downstream. Actually, since the visualized flow-field is 220 mm downstream the rotor, there is a delay between the instant when a vortex is generated and the instant when the same shed vortex reaches the investigation area. For instance, when the rotor is at an azimuth angle $\theta = 126°$, a streamwise velocity peak appears in the investigation windows at the advancing bucket side, which reveal the presence of the vortex shed from the advancing bucket is about an azimuth angle $\theta = 90°$. The streamwise velocity are constantly higher on both sides of the rotor, whereas wind speed is particularly low behind the rotor. However, the streamwise velocities are

generally higher on the advancing bucket side (x values negative) with respect to the returning bucket side (x values positive) due to the circulation produced by the turbine revolution. The low speed area on the back of the rotor is characterized by an evident unsteadiness due to the bucket passage. Even though the Savonius rotor is characterized by a 180° periodicity, the flow-field evidences some discrepancies (for instance compare either the visualizations at 0° and at 180° or the visualizations at 90° and at 270°) making the fluid-dynamic behavior of the rotor periodic only over an entire revolution.

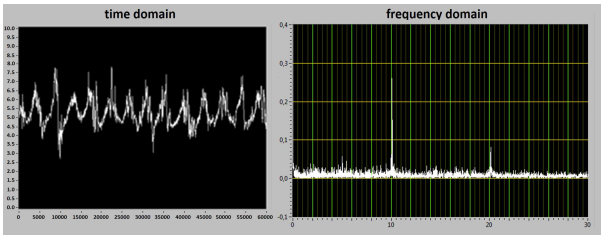

Fig. 11. Velocity in the time and frequency domains during a single continuous acquisition at a defined test node

5. Conclusions

A two-bucket Savonius rotor prototype, obtained from a *PVC* pipe, has been tested inside the closed loop, subsonic, wind tunnel at the Department of Mechanics, Mathematics and Management (*DMMM*) of the Politecnico di Bari. Results have been given in terms of turbine performance and flow-field analysis. In a wide range of tip speed ratios (from 0.3 up to 1.5), the torque coefficient shows a linear dependence with respect to the tip speed ratio, with the highest value at the lowest λ. When considering the polar diagram of the phase-averaged shaft torque, this evidences its typical bilobed shape. However, even if the rotor is characterized by a geometrical symmetry of 180°, this is not the case for the shaft torque coefficient characterized by a lack of periodicity every half revolution due to the complex interaction of the vortex shedding with the rotating buckets. Averaged flow field analyses upstream and downstream the rotor have been performed. Furthermore, the wake downstream of the Savonius rotor has been described. From phase-averaged visualization, the main flow characteristics have been described and the lack of a perfect 180° periodicity in the turbine behavior has been again put in evidence.

References

[1] Global wind energy outlook 2012. Press release of Global Wind Energy Council (*GWEC*).
[2] Global wind report - Annual market update 2012. Press release of Global Wind Energy Council (*GWEC*).
[3] Wind in power 2012 European statistics, February 2013. Press release of European Wind Energy Association (*EWEA*).
[4] Small Wind World Report 2013. Press release of World Wind Energy Association (*WWEA*).
[5] Menet, JL, 2002. Local production of electricity with a small Savonius rotor. In: Proceedings of the 2002 Global Wind Power Conference, April 25, Paris, France.
[6] Savonius SJ. The S-rotor and its applications. Mech Eng. 1931; 53-5: 333-337.
[7] Alexander AJ, Holownia BP. Wind tunnel tests on a Savonius turbine. Journal of Industrial Aerodynamics 1978; 3:343-51.
[8] Fujisawa N, Gotoh F. Visualization study of the flow in and around a Savonius rotor. Experiments in Fluids 1992; 12:407-12.
[9] Fujisawa N. Velocity measurements and numerical calculations of flow fields in and around Savonius rotors. Journal of Wind Engineering and Industrial Aerodynamics 1996;59:39-50.
[10] Torresi M, Fortunato B, Pascazio G, Camporeale SM, 2011. CFD analysis of a Savonius rotor in a confined test section and in open field. In: Proceedings of ASME Turbo Expo 2011: Power for Land, Sea and Air Conference, June 06-11, 2011, Vancouver, Canada.
[11] Valdès LC, Raniriharinosy K. Low technical wind pumping of high efficiency. Renewable Energy 2001; 24:275-301.
[12] Valdès LC, Darque J. Design of wind-driven generator made up of dynamos assembling. Renewable Energy 2003; 28:345-62.
[13] Di Leo L, Design, construction and experimental analysis of a Savonius Rotor. Politecnico di Bari, Graduate thesis, 2010.
[14] Savitzky A, Golay MJE, Smoothing and Differentiation of Data by Simplified Least Squares Procedures. Analytical Chemistry, 1964; 36:1627-39.

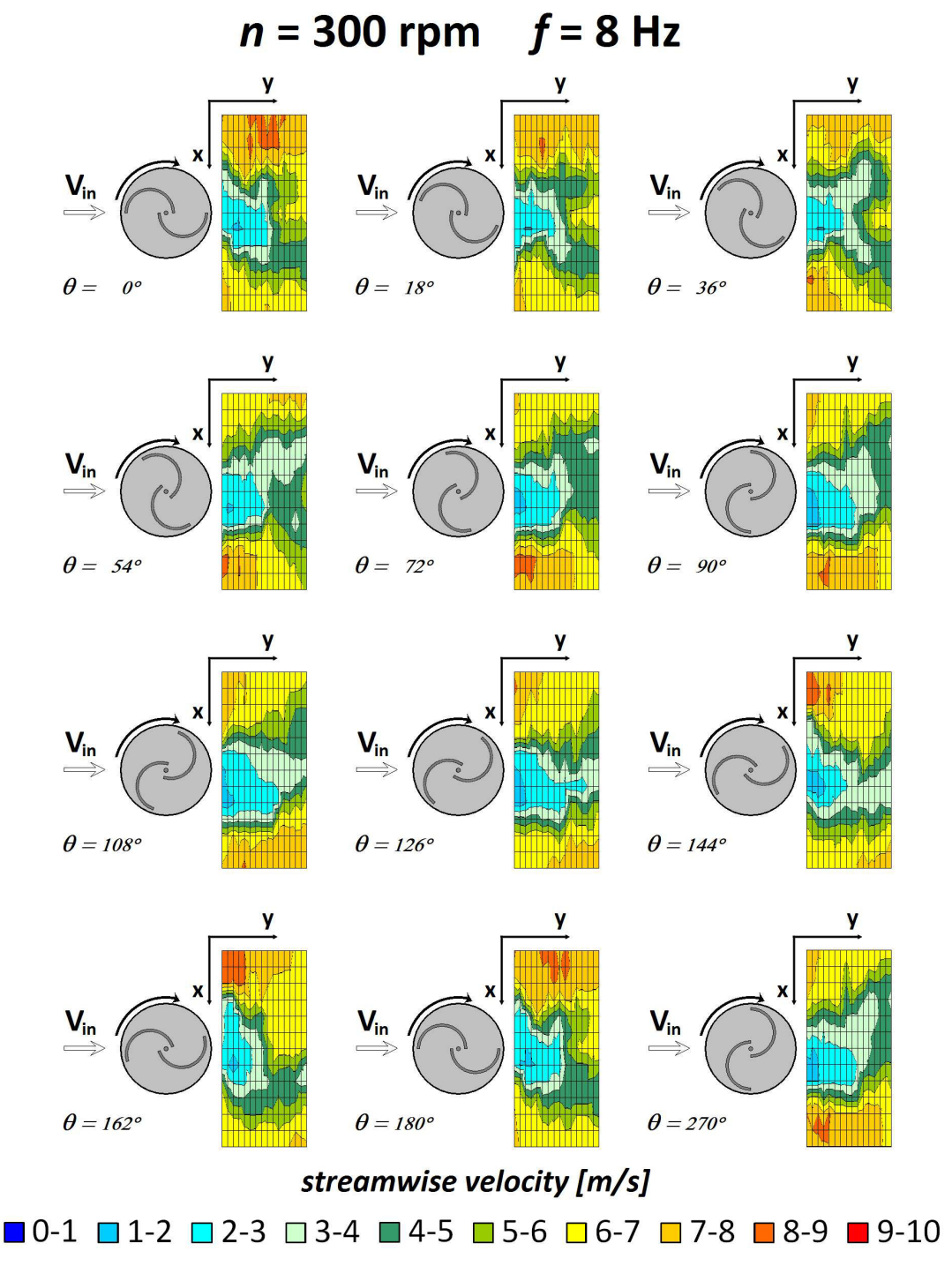

Fig. 12. Phase-averaged flow fields downstream the rotor at $n = 300\,rpm$ and $f = 8\,Hz$ from $\theta = 0°$, up to $\theta = 180°$, every 18°, plus $\theta = 270°$